Supporting Information

Impact of Dispersion Solvent on Ionomer Thin Films and Membranes

Sarah A. Berlinger[1,2,], Peter J. Dudenas[1,2,†], Ashley Bird[1,2], Xunkai Chen[1,2], Guillaume Freychet[3], Bryan D. McCloskey[2], Ahmet Kusoglu[1], Adam Z. Weber[1]*

[1]Energy Conversion Group, Lawrence Berkeley National Laboratory, Berkeley, CA 94720,

[2]Department of Chemical and Biomolecular Engineering, University of California, Berkeley, Berkeley, CA 94720

[3]National Synchrotron Light Source II, Brookhaven National Laboratory, Upton, NY 11973

Corresponding Author

*Sarah A. Berlinger: sarah_berlinger@berkeley.edu

Present Addresses

†Polymer Processing Group, National Institute of Standards and Technology, Gaithersburg, MD, 20899

1. Nafion Structure

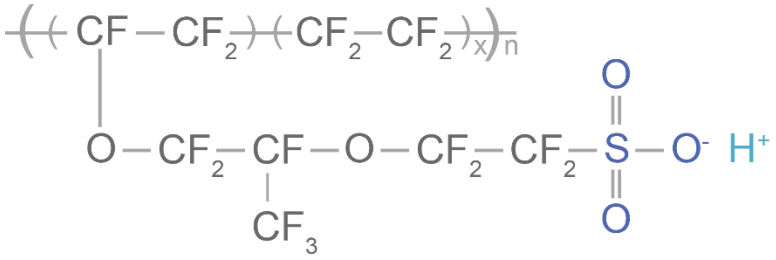

Figure S1. *Structure of Nafion. For an equivalent weight of 1100 g polymer/mol SO_3^- (used in this study), x ~ 6.5.*

2. *In-situ* GISAXS and Dispersion Properties

2.1 Initial Linecuts and Fitting

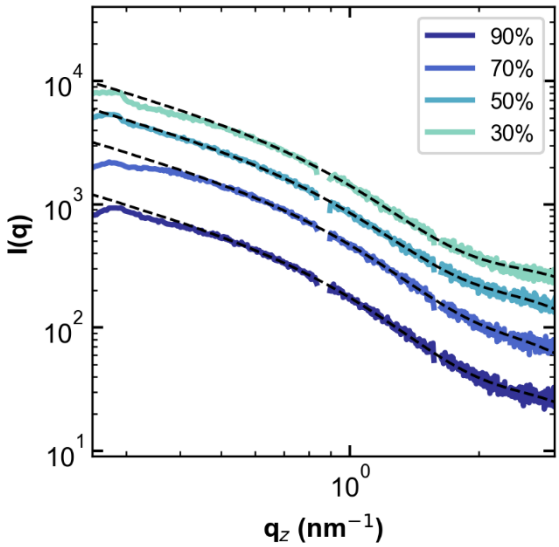

Figure S2.*Through-plane intensity I(q) as a function of q linecuts obtained from GISAXS experiments of the dispersions immediately upon casting. Labels describe the weight percentage of water that makes up the dispersion solvent composition (the balance is n-propanol). Dashed lines show the core-shell form factor fit to the data. Lines are offset from one another for clarity.*

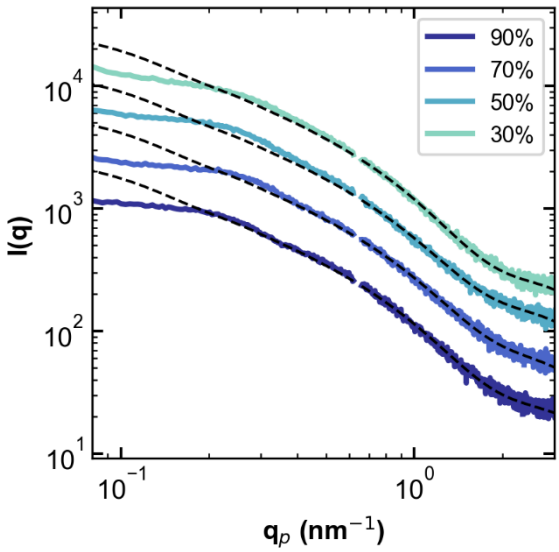

***Figure S3**. In-plane intensity I(q) as a function of q linecuts obtained from GISAXS experiments of the dispersions immediately upon casting. Labels describe the weight percentage of water that makes up the dispersion solvent composition (the balance is n-propanol). Dashed lines show the core-shell form factor fit to the data. Lines are offset from one another for clarity.*

Parameter	30%	50%	70%	90%
Scale (in-plane; through-plane) (a.u)	0.256; 0.303	0.193; 0.301	0.187; 0.341	0.146; 0.234
Core Radius (Å)	8	8	8	8
Shell Thickness (Å)	18.26	19.34	18.61	17.71
Core Length (Å)	400	400	400	400
Core SLD (Å^{-2})	5.05e-5	5.05e-5	5.05e-5	5.05e-5
Shell SLD (Å^{-2})	1.14e-5	1.09e-5	1.09e-5	1.14e-5
Solvent SLD (Å^{-2})	8.79e-6	8.79e-6	8.79e-6	8.79e-6
Background (in-plane; through-plane) (a.u)	5.37; 6.382	4.60; 4.80	3.67; 3.66	3.26; 3.30

***Table S1**. Core-shell form factor fitting parameters.*

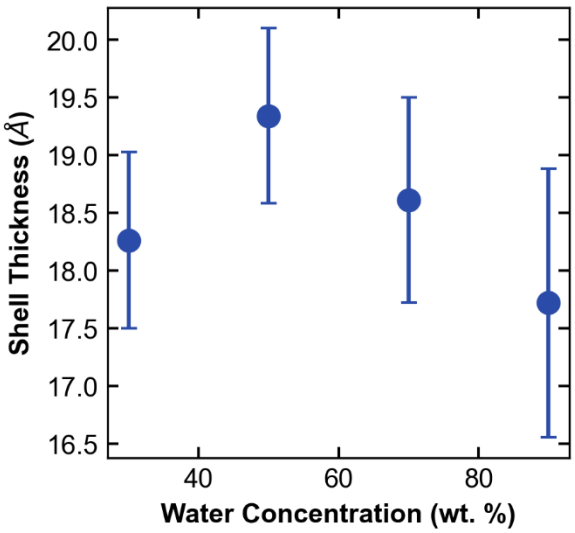

Figure S4. *Shell thickness from core-shell form factor fit of initial linecuts. Error bars represent one standard deviation in fit uncertainty.*

2.2 Structure Factors

The scattering intensity is proportional the electron density contrast, $\Delta\rho$, the structure factor, S(q), and the form factor intensity, P(q).

$$I(q) \propto \Delta\rho^2 P(q) S(q) \tag{S1}$$

where

$$P(q) = \langle |F(q)|^2 \rangle \tag{S2}$$

We define the effective structure factor, $S_{eff}(q)$, as the observed scattering intensity divided by P(q)

$$S_{eff}(q) = \frac{I_{obs}(q)}{P(q)} \tag{S3}$$

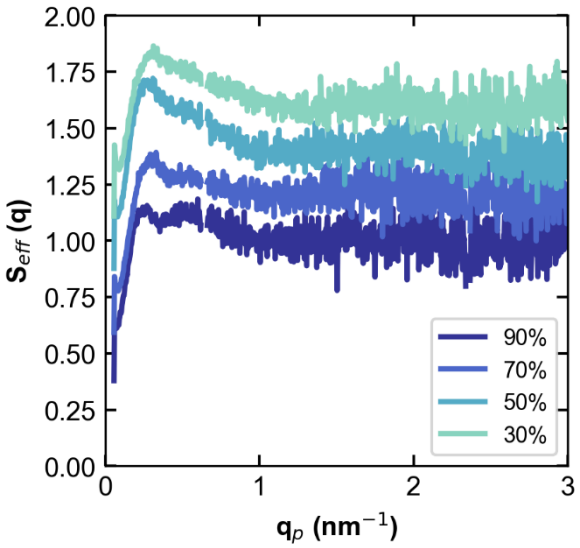

Figure S5. *Initial effective structure factors (S_{eff}) of the dispersions immediately upon casting. This was obtained by dividing the line cuts in Figure 1 (in the main text) by the core-shell form factor. Labels describe the weight percentage of water that makes up the dispersion solvent composition (the balance is n-propanol). Lines are offset from one another for clarity.*

One way to rationalize the two structure factor peaks discussed in the main text is to consider charged-particle aggregation phenomena. Charged particles exhibit heterogeneous aggregation states that can be described by theories such as Two-Yukawa, Darjaguin-Landau-Verwey-Overbeck (DLVO), and others that balance opposing forces such as electrostatic/coulombic repulsion and van der Waals attraction, *etc.*[1] These theories are all characterized by multiple local energy minima in an interaction energy landscape versus particle separation distance, and likely capture the primary physics governing Nafion particle aggregation, at least to a first degree. To summarize qualitatively the resulting energy profiles: the primary energy well at small separation distances governs the internal structure of secondary aggregates (flocs), while the secondary minima at larger separation distances describes separation between discrete aggregates (both secondary and lone primary). The two energy wells are separated by an energy barrier, the height of which dictates whether the primary aggregates can aggregate further (and therefore the stability of the suspension).[1] Within this framework, one can assign the primary structure-factor peak to the secondary energy minima (at larger length scales, smaller q), which describes the arrangement of aggregates in solution (and the characteristic long tail to this minima is indicative of multiple lengthscales/aggregate sizes that this averages over). The secondary structure-factor peak correlates to the primary energy minima (at smaller length scales, larger q). Additional structure-factor modeling work would be required to determine the relative strength of these local minima and how they vary with water:nPA ratio, but this framework provides a qualitative understanding of the data.

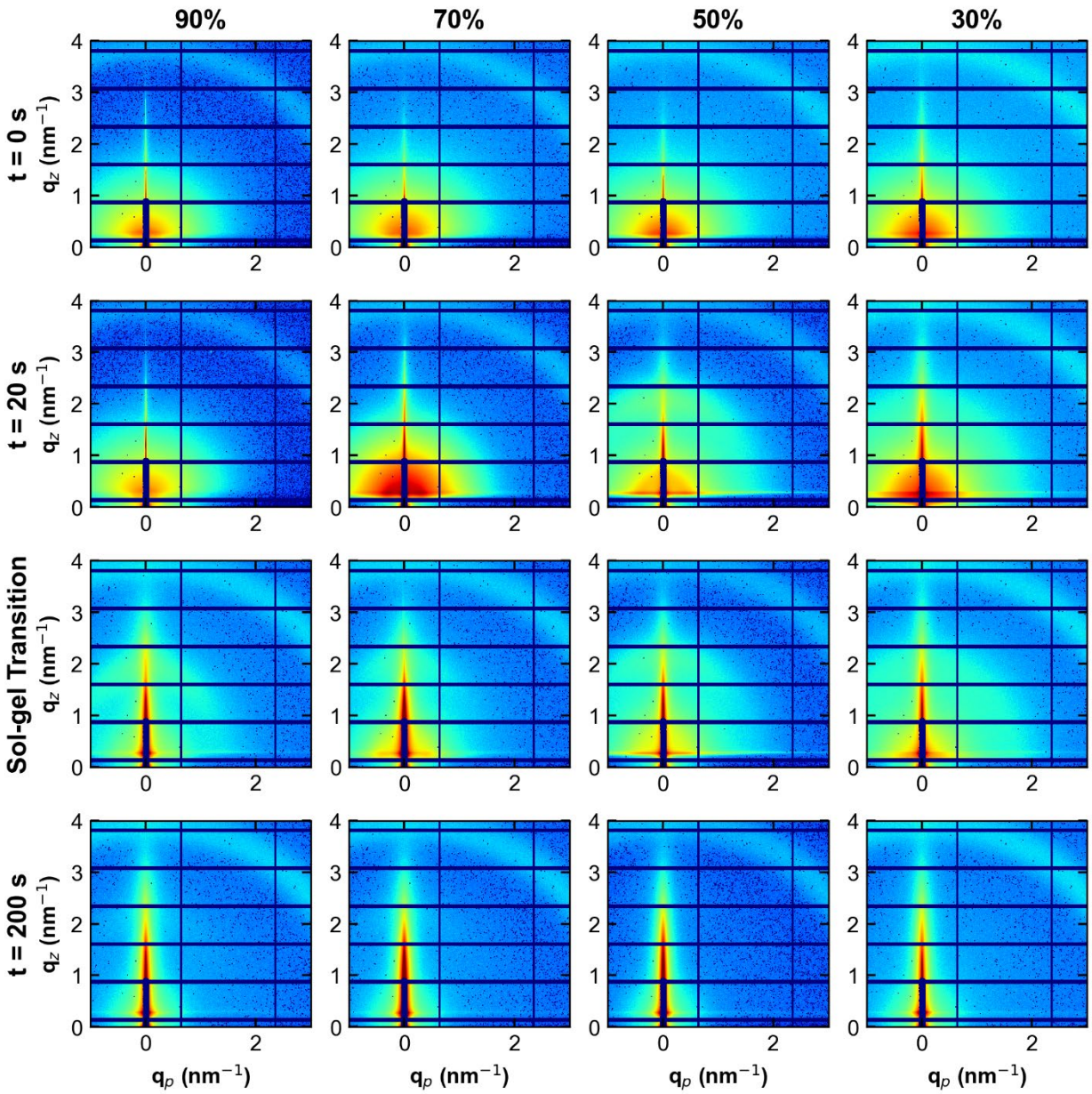

Figure S6. *2D GISAXS images for each water:nPA solvent ratio at select times. The sol-gel transition times shown are 88 s, 42 s, 22 s, and 27s for 90%, 70%, 50%, and 30%, respectively.*

2.3 Rheology

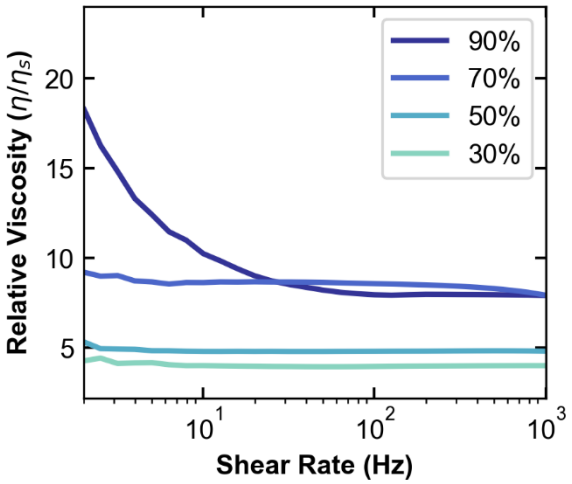

Figure S7. *Measured viscosity of the dispersions (η) divided by the pure solvent viscosity (η_s) as a function of shear rate. Labels describe the weight percentage of water that makes up the dispersion solvent composition (the balance is n-propanol).*

For flow through a slit, the shear rate at the wall ($\dot{\gamma}_{wall}$) is given by:

$$\dot{\gamma}_{wall} = \frac{6Q}{h^2 w} \tag{S4}$$

for a Newtonian fluid.[2] Here, *Q* is the volumetric flowrate, and *h* and *w* are the height and width of the slit, respectively. For the casting experiments, dispersions were printed at a rate of 5 µL/s through a slot-die printer head measuring 1 cm wide by 0.5 cm tall.[3] Even though the dispersions are not perfectly Newtonian, Equation S4 represents a good first approximation to estimate the shear rate experienced by the dispersions during casting experiments, especially for the lower water percentage dispersions. Accordingly, the shear rate is roughly 12 Hz. Data collected at 12.59 Hz (in Figure S7) is presented in the main text in Figure 3.

2.4 Teubner-Strey Fitting

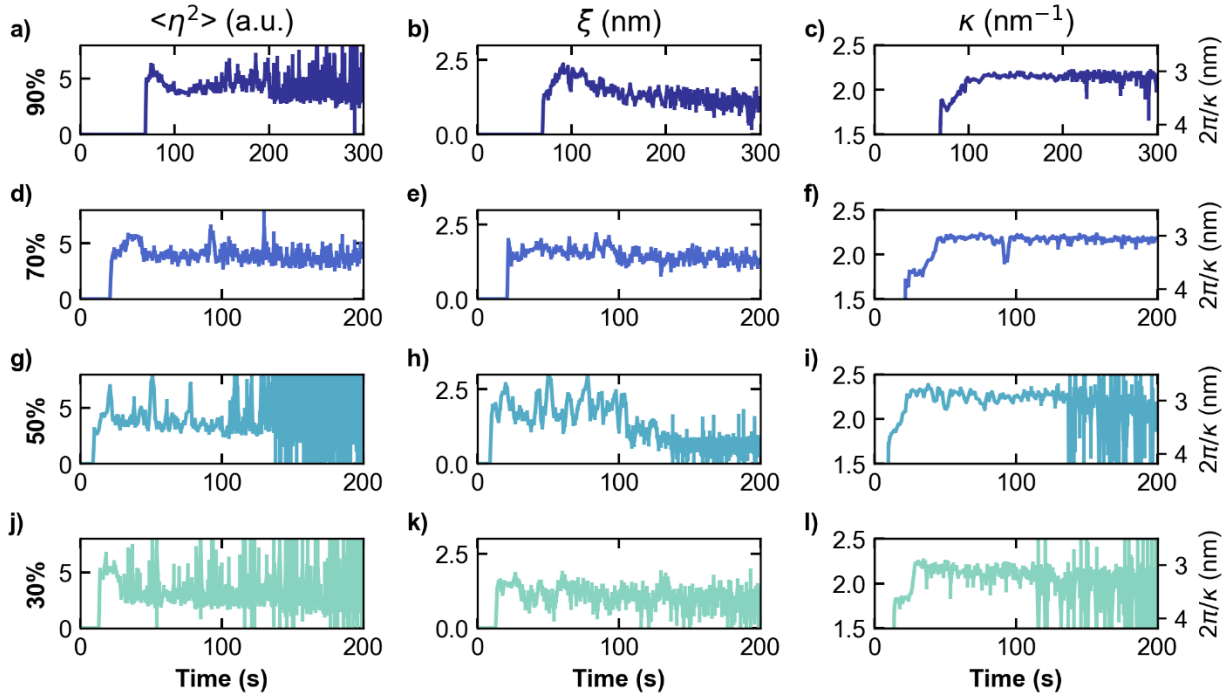

Figure S8. *Gel to final film through-plane Teubner-Strey fitting parameters as a function of time, with error bars. Labels describe the weight percentage of water that makes up the dispersion solvent composition (the balance is n-propanol). Note the 90% goes out to 300 seconds.*

The ionomer peak was fit to the Teubner-Strey Model[4-5]

$$I(q) = \frac{8\pi\langle\eta^2\rangle}{\xi(a - 2bq^2 + q^4} + background \tag{S5}$$

$$a = \left(\kappa^2 + \frac{1}{\xi^2}\right)^2 \qquad b = \left(\kappa^2 - \frac{1}{\xi^2}\right)$$

The fitting parameters are $\langle\eta^2\rangle$, κ, ξ, and background. $\langle\eta^2\rangle$ is a function of volume fractions and the scattering length contrast, κ is inversely related to the spacing between domains, and ξ is the correlation length of domains.

Figure S8 shows parameters of the Teubner-Strey model versus time for the four water:nPA ratios. Both the 30% and 50% water films quickly approach their final parameter values within first 20 seconds after transitioning to the gel state. Between these two films, the 30% water film shows a lower correlation length, ξ, and the fits are considerably noisier because the ionomer peak falls below background. The 50% water film maintains a high correlation length, that oscillates in value through 100s, after which it similarly dries with no visible ionomer peak. The high-water-concentration dispersions (HWD; 70% and 90%), both begin gelation later because of the lower volatility solvent mixture. The HWD maintain a higher correlation length through the drying process and the ionomer peak in both more slowly proceed to their final values.

At t = 200s, the LWD show no visible ionomer peak, while it is still visible in the HWD films. Figure S9 plots the time at which κ and ξ reach what appear to be their equilibrium values. The HWD samples are slowly drying, so ξ may continue to very slowly decay to its final value, but that is beyond the timescale of these experiments.

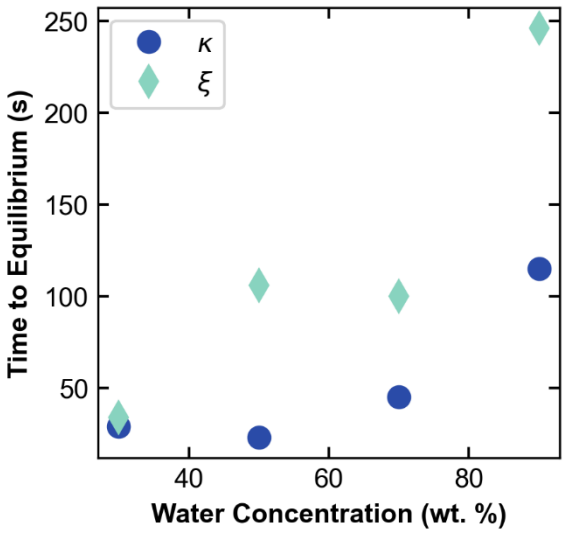

Figure S9. *Time to equilibrium versus weight percentage of water (the balance is n-propanol).*

	30%	**50%**	**70%**	**90%**
Thickness (nm)	93 ± 32	84 ± 16	107 ± 20	159 ± 71

Table S2*. Final film thicknesses of the dried films from the casting experiments as measured by ellipsometry. At least 7 points are averaged over the width of the film.*

3. Membrane Structure and Properties

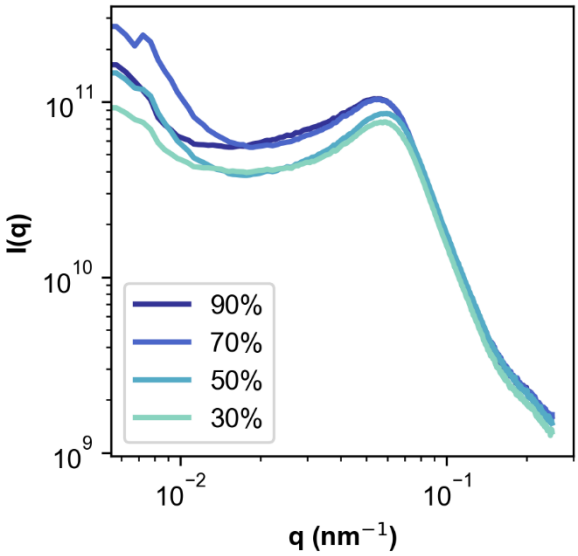

Figure S10. *Inter-crystalline WAXS peak of the membranes at 2452 eV. Labels describe the weight percentage of water that makes up the dispersion solvent composition (the balance is n-propanol).*

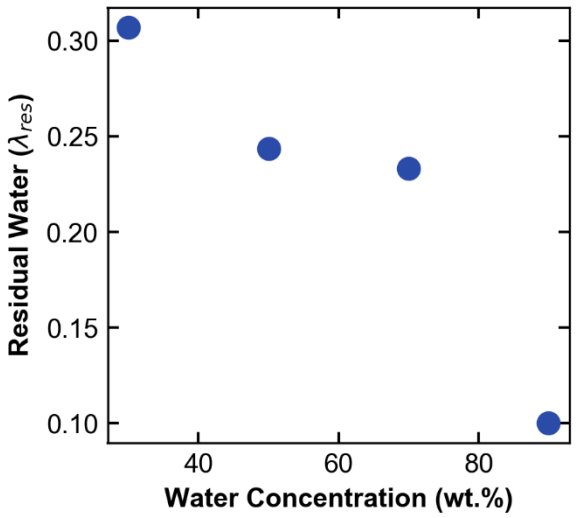

Figure S11. *Residual water from membrane swelling measurements, as a function of the dispersion water concentration (balance n-propanol) from which the membranes were cast.*

4. References

1. Israelachvili, J. N., *Intermolecular and Surface Forces*. Academic Press: 2011; Vol. 3.
2. Bird, R. B.; Stewart, W. E.; Lightfoot, E. N., *Transport Phenomena, Second Edition*. John Wiley & Sons, Inc.: 2002.
3. Liu, F.; Ferdous, S.; Schaible, E.; Hexemer, A.; Church, M.; Ding, X.; Wang, C.; Russell, T. P., Fast printing and in situ morphology observation of organic photovoltaics using slot-die coating. *Advanced materials (Deerfield Beach, Fla.)* **2015,** *27* (5), 886-91.
4. Teubner, M.; Strey, R., Origin of the scattering peak in microemulsions. *The Journal of Chemical Physics* **1987,** *87* (5), 3195-3200.
5. Chen, S. H.; Chang, S. L.; Strey, R. In *On the interpretation of scattering peaks from bicontinuous microemulsions*, Darmstadt, Steinkopff: Darmstadt, 1990; pp 30-35.